DOI 10.4430/bgo00369

# Investigation of shoreline change rates using the digital shoreline analysis system in Lake Beyşehir, Turkey

M.G. Gümüs[1], S.S. Durduran[2] and K. Gümüs[1]

[1] *Department of Geomatics Engineering, Faculty of Engineering, Niğde Ömer Halisdemir University, Niğde, Turkey*

[2] *Department of Geomatics Engineering, Faculty of Engineering, Necmettin Erbakan University, Konya, Turkey*

(Received: 15 February 2021; accepted: 22 July 2021; published online: 3 December 2021)

***ABSTRACT*** This study was aimed to investigate the temporal and geometric shoreline change rates in Lake Beyşehir, which is the largest freshwater lake in Turkey, using the Digital Shoreline Analysis System and remote sensing techniques. Therefore, the multitemporal Landsat satellite images for 1984, 1990, 1996, 2000, 2006, 2014, and 2018 were used. The shoreline maps of the study area were produced from the obtained satellite images, and the shoreline change rates for the previous years were calculated using two different methods. As a result of the study, according to the end point rate and linear regression rate statistics, the highest average coastal erosion rate was determined to be -12.03 m/yr with shoreline withdrawal of 409.06 m in a 35-year period, and the highest average coastal accretion rate was determined to be 5.86 m/yr with shoreline advance of 178.36 m. In addition, trend and drought analyses were applied to the annual average meteorological data (temperature and precipitation) from 1970 to 2018, which were obtained from the Beyşehir Meteorological Observation Station located in the study area. The results of these analyses were used to determine whether the temperature and rainfall changes over the years have had an effect on the temporal and geometric coastline changes in Lake Beyşehir.

**Key words:** accretion and erosion, DSAS, EPR, LRR, shoreline change, trend analysis.

## 1. Introduction

Shorelines are dynamic environments that separate terrestrial from marine ones (Lutgens *et al.*, 2012; Kadıoğlu *et al*., 2019). Coastal areas are one of the most complex ecosystems, with many living and inanimate resources (Constanza *et al*., 1997; Kuleli, 2010). Therefore, coastal areas are defined as dynamic regions of great importance for sustainable land management practices. These areas, which are very sensitive for sustainable land management, are endangered due to: natural reasons, such as coastal erosion; meteorological, hydrological, and geological factors, that cause land degradation; and artificial reasons, including coastal engineering, land demand, and agricultural activities (Mohsen *et al*., 2018; Dereli and Tercan, 2020).

Another important factor is the effect of climate change, especially drought. The effects of the climate changes that have been experienced in the climate zone in which Turkey is located include sudden fluctuations in precipitation and temperatures, and decreased water resources,

which have resulted in a decrease in productivity in agricultural activities. Nowadays, the adverse effects caused by climatic changes have been defined as an important factor that threatens our future. Possible scenarios that will occur in Turkey, and especially in the Mediterranean Basin, according to the 5th Assessment Report (AR5) published by the Intergovernmental Climate Change Panel (IPCC) in 2013, have revealed the seriousness of the situation.

As one of the inland wetlands, lakes are living areas that have critical importance for the sustainability of living ecosystems, as these regions are structures with high nutritional value for living things, and they host many species (Dereli and Tercan, 2020). Lakes also serve as a resource for people. Their use for various reasons, such as agricultural activities, energy production, tourism, and drinking water, gradually decrease their water reserves, which creates a problem for inland wetlands.

For this reason, understanding the dynamic structure of the shoreline and investigating temporal changes quantitatively are extremely important for making effective decisions regarding coastal management (Esteves *et al*., 2009; Rio *et al*., 2013). Remote Sensing (RS) and geographic information system (GIS) technologies are frequently used nowadays in the determination of coastal changes and future trends, in various planning activities and preventive studies, due to the fact that the use of classical methods creates disadvantages in terms of time, cost, and benefits (Thanikachalam and Ramachandran, 2003; Navrajan *et al*., 2005; Pepe and Coutu, 2008; Pritam and Prasenjit, 2010; Natesan *et al*., 2013; Bheeroo *et al*., 2016; David *et al*., 2016; Duru, 2017).

GIS and RS techniques are used as very important tools in the planning and analysis of natural resources in terms of time and precision. These technologies provide quickness and flexibility in making decisions for users and decision-makers. RS plays an essential role in economical spatial data acquisition (Alesheikh *et al*., 2007), making digital images simple to interpret and easy to obtain. Furthermore, the absorption of the infrared wavelength region, by water and its strong reflection by vegetation and soil, make these images an ideal combination to map the spatial distribution of terrestrial and marine areas (Niya *et al*., 2013). Hence, images containing visible and infrared bands are commonly used for shoreline mapping. Two methods are usually used when making shoreline extractions with RS data. The first of these is the digitisation conducted on the screen, as its margin of error is less. The second is the automatic method, in which extraction is performed using different algorithms according to the software and the data are used in a comparison with the previous method (Chen and Rau, 1998; Frazier and Page, 2000; Ryu *et al*., 2002). Although this method saves time, cost, and workforce, its accuracy may vary according to the method and algorithm used. The GIS provides convenience to the user in classification studies, temporal change detection, collecting data in a specific database, analysing, mapping, and in its presentation to the user.

There are different techniques used for measuring and proportioning the temporal and geometrical changes of coastal changes. The Digital Shoreline Analysis System (DSAS) tool, which works as an extension of the ArcGIS software used in the GIS and RS analysis processes, has recently been preferred in coastal survey studies (Ahmad and Lakhan, 2012; Bheeroo *et al.*, 2016; Baral *et al*., 2018; Esmail *et al*., 2019; Hovsepyan *et al*., 2019; Nassar *et al*., 2019). These studies regarding lakes in Turkey are quite limited (Kuleli, 2010; Kuleli *et al*., 2011; Duru, 2017; Kale, 2018; Dereli and Tercan, 2020).

The goal of this study was to investigate the temporal and geometric shoreline changes, and erosion and accretion risk ratio in Lake Beyşehir, which is the largest freshwater lake in Turkey, using the RS technique and the DSAS tool. For this purpose, multiband Landsat Thematic Mapper (TM), Enhanced TM (ETM), and Operational Land Imager (OLI) satellite images for 1984, 1990,

1996, 2000, 2006, 2014, and 2018 were used. Raw satellite images were first atmospherically rectified using image pre-processing techniques on the satellite images. The shoreline was extracted by separating the boundary between terrestrial and marine using the band ratio technique on the obtained images. Shoreline maps were produced from the data obtained, and the shoreline change rates for the previous years were calculated using two different statistical methods, and then the obtained results were analysed. Finally, drought and trend analysis was applied to determine whether the temporal and geometrical changes of the coastline in Lake Beyşehir have temperature and rainfall effects in the years. For this purpose, the annual average meteorological data (temperature and precipitation) for 1970 to 2018, obtained from the Beyşehir Meteorological Observation Station in the study area, were analysed. The Mann-Kendall and Sen Slope tests were used in determining the trends with the temperature and precipitation data, and the Standard Precipitation Index (SPI) was used in determining drought periods only for the rainfall data.

## 2. Material and methods

### *2.1. Study area*

Lake Beyşehir, the third largest lake after lakes Van and Tuz in Turkey, is located between 38°03' and 37°26' N latitude and 31°46' and 31°15' E longitude in the Lakes District (Fig. 1). The Beyşehir-Kaşaklı sub-basin is spread across a wide area of 7391 km$^2$, including the provinces of Konya and Isparta, and non-settled areas of the province of Antalya. Due to its location, the basin exhibits a transition climate, which includes the features of the Mediterranean and terrestrial climates. For this reason, the vegetation part in the basin shows diversity.

The lake is a source of drinking-usage and irrigation water for central Anatolia (Durduran and Çiftçi, 2008). Since the lake is a reservoir of drinking water, it is subject to the Water Pollution Control Regulation. It has a surface area of approximately 650 km$^2$. The lake is very shallow, with an average depth of 8.5 m, with a maximum of 10 m (Tüstaş, 1999). The area was declared as a National Park by the Ministry of Forestry in 1993 under two separate names, Beyşehir Lake and Kızıldağ National Park. Furthermore, it is a wetland area with international importance according to the Ramsar Convention criteria. Lake Beyşehir and its surroundings comprise a very important region in terms of cultural and historical heritage, which is under protection as 1st-, 2nd-, 3rd-Degree Natural Protected Areas. In addition to all of these, the Konya Closed Basin constitutes 14% of the land potential of Turkey in terms of agricultural production (Orhan, 2014). However, due to the unconscious and wild irrigation activities used in agriculture, arid lands prone to desertification are increasing as a result of the overloading of underground and existing water resources.

The main reason for selecting Lake Beyşehir as a study area was the fact that it is an important basin on which emphasis should be placed due to the following factors: the increasing agricultural irrigation activities and unconscious water use; it is the largest freshwater source in Turkey; sudden changes in precipitation and temperature have resulted in increased drought waves; the drying of most of the 27 creeks and streams feeding the lake; the pollution caused by the increasing discharge of domestic and industrial wastes into the lake; the decreased biodiversity in the lake; the increasing coastal erosion; and, consequently, the physical and human-induced changes, such as irregular change activities along the shore border. The fact that the region is facing drought and that its location in the basin is most affected by climate

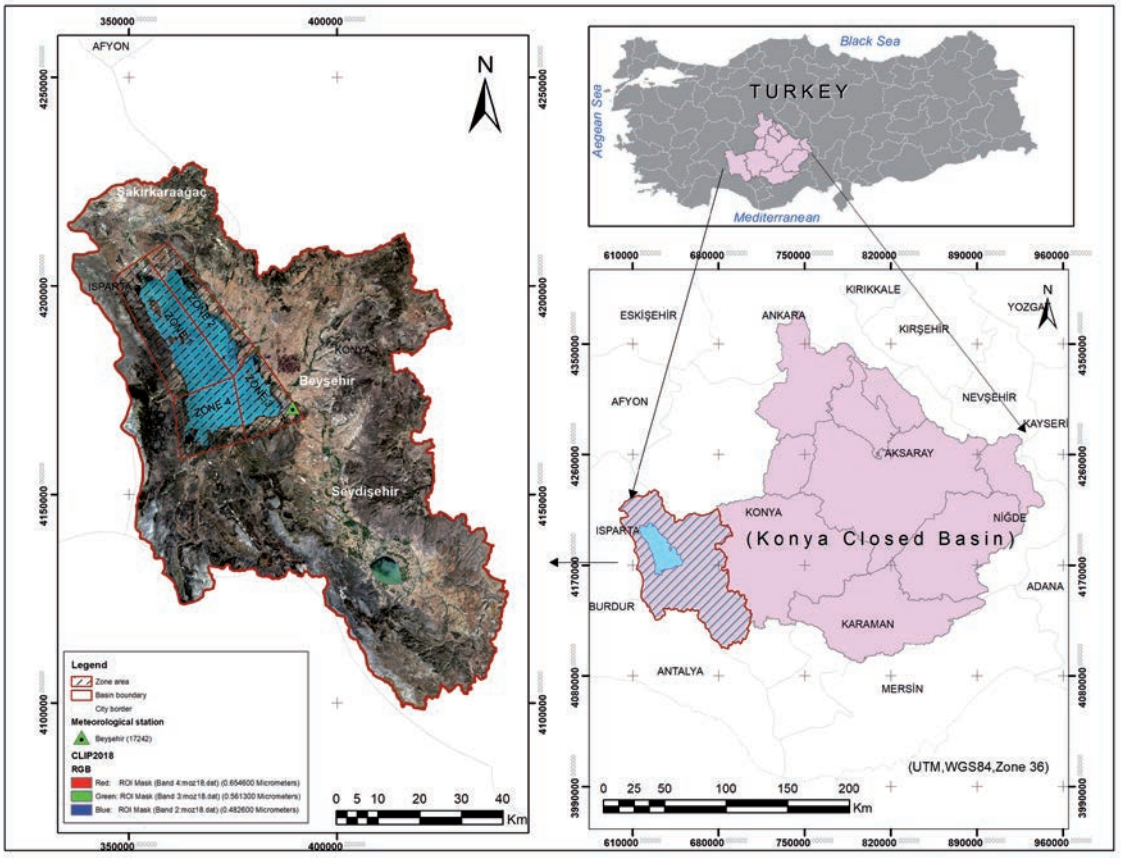


Fig. 1 - Location of the study area (Landsat-8 OLI, RGB image data, 2018).

change in Turkey was also effective in determining the study area. Furthermore, when the management plan analysis reports related to the management of the surface water of Lake Beyşehir were examined, it was decided to select it as the study area due to the absence of a comprehensive study on the subject and the lack of inventory data for the region to be used as a base.

## *2.2. The used data*

In this study, the Landsat TM, ETM, and OLI digital satellite images for 1984, 1990, 1996, 2000, 2006, 2014, and 2018 were used. Landsat satellite images were used in the present study due to the presence of a large data archive, their having a medium spatial resolution (30×30), being frequently preferred in the determination of environmental changes, providing sufficient information in the wide application area, and being served free of charge. The Landsat satellite images used in the study were provided by the United States Geological Survey (USGS) Research Institute website (United States Geological Research Institute, 2020).

Landsat 5 TM, 7 ETM, and 8 OLI satellites take images in the visible and near-infrared (VNIR), shortwave infrared (SWIR), and thermal infrared (TIR) ranges, and have a medium spatial resolution that is between 15 and 100 m, depending on the spectral range. Their lane widths

are 183, 185, and 185 km, respectively, and their temporal resolution is 16 days. Their spatial resolution spectral bands are 30 m, their radiometric resolution is 8 bits, and they orbit at an altitude of 705 km. Different than Landsat 5, Landsat 7 has a developed thematic mapper scanner. In addition to the standard 7 bands, a panchromatic band (0.50-0.90 μm) with a 15-m resolution was added. In addition to these, the resolution of the thermal band was reduced from 120 to 60 m. Landsat 8, which joined the trajectory of Landsat 7 in 2013, provides scientific data. In addition to the previous bands, Landsat 8 OLI carries a deep blue band for coastal/aerosol studies, as well as a short wave infrared band for the detection of cirrus clouds. OLI collects data as 9 spectral bands (Coastal/Aerosol + VNIR + SWIR + PAN + CIRRUS), and of these, 7 have the ranges found in the previous LANDSAT 5 TM and 7 ETM sensors; thus, compatibility with old Landsat data is ensured. The technical characteristics of the Landsat satellite images used in the study are presented in Table 1.

Table 1 - Used satellite images and technical specifications.

| No | Spacecraft_Id | Sensor | Path / Row | Spatial resolution | Date acquired | Type |
|---|---|---|---|---|---|---|
| 1 | Landsat 5 | TM | 178/34 | 30 m | 1984-07-16 | GeoTiff |
| 2 | Landsat 5 | TM | 178/34 | 30 m | 1990-08-02 | GeoTiff |
| 3 | Landsat 5 | TM | 178/34 | 30 m | 1996-08-02 | GeoTiff |
| 4 | Landsat 7 | ETM | 178/34 | 30 m | 2000-08-05 | GeoTiff |
| 5 | Landsat 5 | TM | 178/34 | 30 m | 2006-08-30 | GeoTiff |
| 6 | Landsat 8 | OLI | 178/34 | 30 m | 2014-07-03 | GeoTiff |
| 7 | Landsat 8 | OLI | 178/34 | 30 m | 2018-08-15 | GeoTiff |

ENVI 5.3 software (Exelis Visual Information Solutions, Boulder, CO, USA) was used in the digital pre-processing of satellite images and determining the border between terrestrial and marine sea using the band ratio technique. In order to extract the border from the resulting images, raster-to-vector conversion processes were used, and ArcGIS 10.5 software (Environmental Systems Research Institute, Redlands, CA, USA) was used in all visualisation and mapping stages, and the DSAS 5.0 tool, which runs as an extension of the ArcGIS software, was used in the statistical determination of the shoreline change rates.

In addition, monthly and annual average meteorological data (temperature and precipitation) for 1970 to 2018, obtained from the Beyşehir Meteorological Observation Station in the study area, were used to determine whether the temperature and rainfall affected the interpretation of the temporal and geometrical coastal changes in Lake Beyşehir. The Beyşehir meteorology station was chosen because it is the closest to this lake and has at least 30 years of meteorological data for the trend analysis. Related data were obtained from the General Directorate of Meteorology in Turkey. The average annual values were found by taking the averages of the months covering that year for each year in a time series of different data types for 1970 to 2018. Time series were created for the temperature and precipitation data for the trend analysis. Descriptive statistics for the annual average of these time series are given in Table 2. In addition, monthly and precipitation data for these years were used to determine the drought periods. The monthly average values of the data obtained from the Beyşehir station are given in Table 3.

Table 2 - Annual average values obtained from Beyşehir station. N: number of year, min.: minimum value, max.: maximum value, std. dev.: standard deviation.

| Meteorological | Beyşehir Station | | | | |
|---|---|---|---|---|---|
| Data | N | Min. | Max. | Mean | Std. Dev. |
| Minimum Temperature | 49 | -3.75 | 0.45 | -1.32 | 1.05 |
| Average Temperature | 49 | 8.35 | 13.03 | 10.85 | 0.82 |
| Maximum Temperature | 49 | 21.6 | 25.93 | 23.31 | 0.97 |
| Total Precipitation | 49 | 26.64 | 56.01 | 41.21 | 7.39 |

Table 3 - Monthly average values obtained from Beyşehir station.

| Beyşehir Meteorological Data | Jan. | Feb. | Mar. | Apr. | May | June | July | Aug. | Sep. | Oct. | Nov. | Dec. |
|---|---|---|---|---|---|---|---|---|---|---|---|---|
| **Min. temperature** | -12.5 | -12.3 | -7.5 | -1.6 | 2.8 | 6.6 | 10.2 | 9.5 | 5.0 | 0.0 | -5.6 | -10.4 |
| **Average temperature** | -0.3 | 1.0 | 5.1 | 10.0 | 14.5 | 18.6 | 22.0 | 21.8 | 17.8 | 12.0 | 6.0 | 1.6 |
| **Max. temperature** | 11.2 | 13.4 | 18.7 | 23.6 | 27.3 | 31.0 | 33.5 | 33.4 | 30.6 | 25.5 | 18.3 | 13.3 |
| **Total precipitation** | 70.4 | 48.0 | 46.7 | 44.9 | 42.8 | 27.0 | 9.2 | 10.8 | 19.6 | 47.3 | 55.0 | 72.9 |

### 2.2.1. Correlation analysis

Correlation analysis was conducted to determine the direction and magnitude of the relationship between temperature and precipitation data observed from the Beyşehir station. Nonparametric Spearman's Rho correlation analysis was applied to these data, since some of the data did not show normal distribution and were not homogeneous (Table 4). The correlation coefficient (*r*) is a parameter that takes values between -1 and 1, which measures the direction and amount of the linear relationship between two variables. As the value of *r* approaches 0, the dependency can be considered very little or absent. It is accepted that *r* has a positive (+) relationship between 0 and 1. It is accepted that *r* has a negative (-) relationship between 0 and -1.

Table 4 - Nonparametric Spearman's Rho correlation analysis results.

| Spearman's rho correlations | | | | |
|---|---|---|---|---|
| **Beyşehir** | **minimum** | **average** | **maximum** | **total** |
| **Meteorological Data** | **temperature** | **temperature** | **temperature** | **precipitation** |
| **Minimum** | 1.000 | 0.771** | 0.254 | 0.154 |
| **temperature** | | 0.000 | 0.078 | 0.290 |
| **Average** | 0.771** | 1.000 | 0.556** | 0.345* |
| **temperature** | 0.000 | | 0.000 | 0.015 |
| **Maximum** | 0.254* | 0.556** | 1.000 | 0.158 |
| **temperature** | 0.078 | 0.000 | | 0.279 |
| **Total** | 0.154 | 0.345* | 0.158 | 1.000 |
| **precipitation** | 0.290 | 0.015 | 0.279 | |

** Correlation is significant at the 0.01 level. * Correlation is significant at the 0.05 level.

## 2.3. Methods

In this study, RS, GIS, and DSAS technologies were used as an effective platform to evaluate shoreline changes on the shores of Lake Beyşehir between 1984 and 2018. The workflow diagram of the study is shown in Fig. 2.

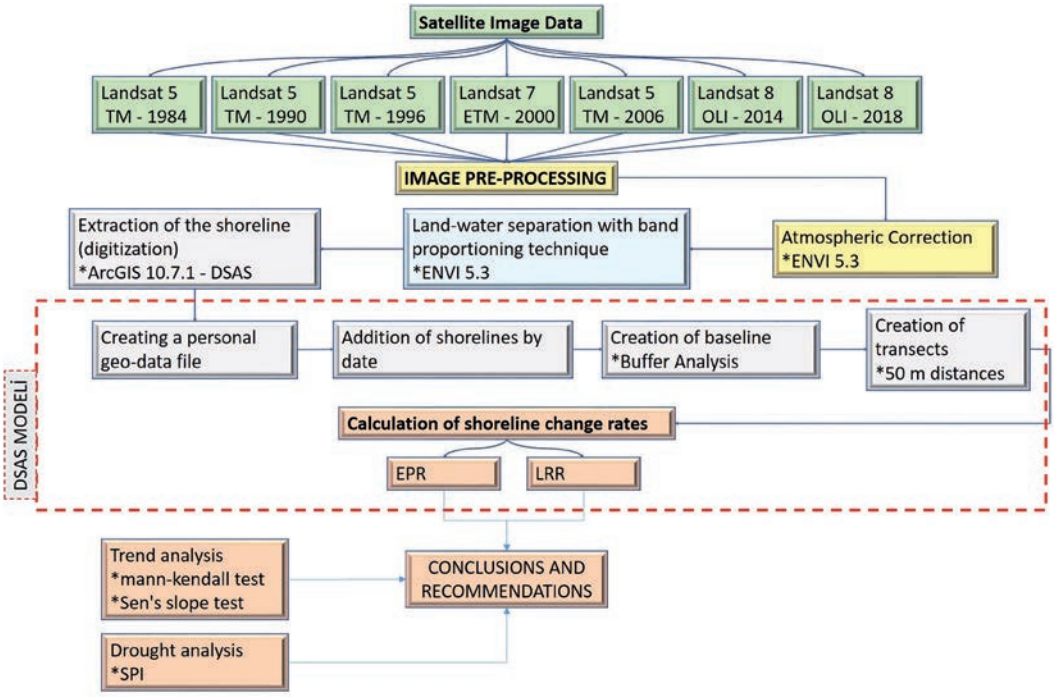


Fig. 2 - Work flow diagram.

### 2.3.1. Image pre-processing

Satellite images contain systematic or non-systematic errors in their structure. Therefore, any existing errors (image pre-processing) should be corrected before using the images. The Landsat satellite images for the 7 years to be used in this study were first rectified by performing their radiometric calibrations. The Landsat image data were downloaded in the corrected level1 GeoTiff (Geo-referenced Tagged Image File Format) format so as to eliminate the need for geometric correction.

### 2.3.2. Extraction of shorelines

After pre-processing of the Landsat satellite images of Lake Beyşehir, the shoreline maps of the study area for different dates were produced. The extraction of the boundary line between terrestrial and marine is based on the development of the spatial and spectral properties of satellite images (Kaliraj *et al*., 2014). Various techniques and methods have been developed to extract the shoreline from RS images. In addition to advanced feature extraction algorithms for the automatic extraction of shorelines, digitisation, band ratio, edge detection and supervise and unsupervised classification techniques using single or multiple bands (Braud and Feng, 1998; Mas, 1999; Bagli and Soille, 2003; Li *et al*., 2003; Liu and Jezek, 2004; El Banna and Hereher,

2009; Kumar *et al*., 2010; El-Asmar and Hereher, 2011; Pardo-Pascual *et al*., 2012) are the most common techniques for the extraction of shorelines, in the literature.

In the current study, the band ratio technique was used to extract the shoreline from remotely sensed images. This is an image processing technique used to determine some properties (vegetation detection, terrestrial and marine separation, marshland separation, etc.) that cannot be determined in raw images. Ratio images are used for the extraction and mapping of coastal changes in different regions by enhancing spectral contrasts between bands (Segal, 1983; Kenea, 1997). Band ratio is performed to clarify differences in the terrestrial and marine separation by dividing the band with high reflectance in a certain spectral range by the band with low reflectance (absorption). The value of each pixel with high reflectance in an image is divided by the value of the pixel in the same position in the band with low reflectance (Kayadibi and Aydal, 2013). In RS images, the green band (VIR) and near-infrared band (NIR) are usually used in the detection of open water surfaces. The effect of soil and settled land is reduced by replacing the NIR band with the Short-wave Infrared (SWIR), and it is possible to obtain a more dominant image by enhancing water extraction. In this study, in order to perform terrestrial and marine boundary separation, the 'band5/band2' ratio was applied to the TM and ETM satellite images, and the 'band6/band3' band ratio technique was applied to the OLI satellite images. As a result of the band ratio technique, binary images providing terrestrial and marine boundary separation were obtained (Fig. 3). The formula used was in the form of "If B5/B2 < 1 then 255 else 0 algorithm" for the Landsat 5 TM and 7 ETM satellite images, and in the form of "If B6/B3 < 1 then 255 else 0 algorithm" for the Landsat 8 OLI satellite images. Here, the green band (0-0.60 nm) was expressed as B2 for TM/ ETM images, and B5 was expressed as SWIR (1.55-1.75 nm). For the OLI satellite image, the green and SWIR bands were B3 and B6, respectively. The raster-vector conversion was performed using the ArcGIS software to extract coastal lines from the resulting images (binary image), where the terrestrial and marine separation can be clearly distinguished.

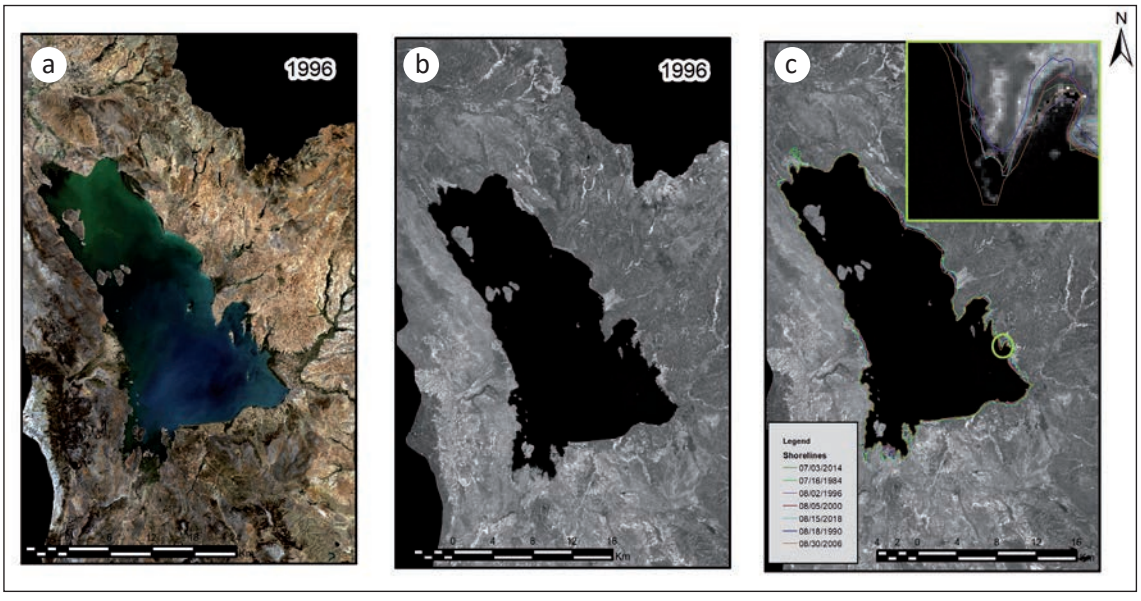


Fig. 3 - Coastline extraction using the band ratio technique for the Landsat TM, ETM, and OLI images: a) overlaying the extracted coastline with the true colour composite ETM image, 1996; b) result of the "If B5/B2 < 1 then 255 else 0 algorithm", binary image; c) extraction of the coastline vector information and raster-to-vector conversion.

### 2.3.3. Calculation of shoreline changes

After extracting the shoreline from the Landsat TM, ETM, and OLI images, the DSAS software tool was used to calculate the shoreline movement rate and changes. DSAS 5.0 is a tool that runs as an add-on to the ArcGIS software (Jayson-Quashigah *et al*., 2013; Kılar and Çiçek, 2018). DSAS (Thieler *et al*., 2003) is a free service application that calculates the statistical changes of many shoreline positions and has been frequently used in the literature (Kuleli *et al*., 2011; Moussaid *et al*., 2015; Mutaqin, 2017; Kale *et al*., 2019). DSAS creates cross-sections (transects) perpendicular to a user-specified baseline. Afterward, the cross-sectional positions of the shoreline along the baseline are recorded (Himmelstoss, 2009; Ali and Narayana, 2015). To evaluate the temporal and geometric change movement of the shoreline, buffer analysis (200 m) was applied to these layers after the shorelines were formed. In this way, a hypothetical baseline was created. The distance measured between the fixed baseline point and the shoreline locations generated by the program provided a reliable record that tracked changes in the shoreline locations over the 35-year time frame of the created vectors. In this study, 3342 transects were produced perpendicular to the baseline at 50 m intervals to the shoreline (Fig. 4). These created transects

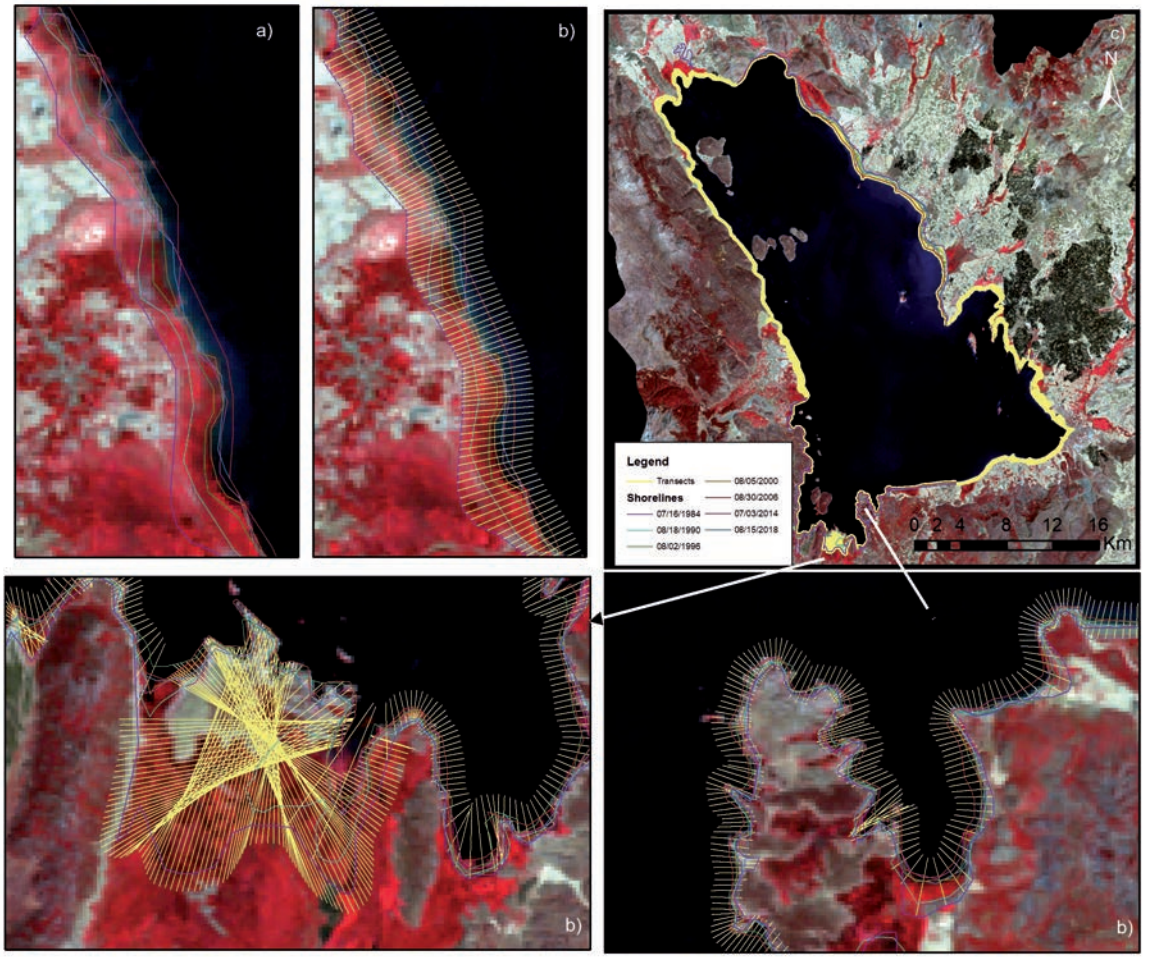


Fig. 4 - Display of the transects (Landsat-5 TM, False colour image data, 1996): a) zooming in of the shoreline changes by year; b) zooming in of the transects; c) display of the transects and shoreline changes by year.

covered the entire study shoreline of Lake Beyşehir (approximately 176 km in length). The data measured from each transect point were then used to predict the annual average rate (m/yr) of the shoreline change using linear regression techniques (Kuleli, 2010).

There are many methods to analyse the rate of shoreline changes, some of which are as follows: Shoreline Change Envelope (SCE), Net Shoreline Movement (NSM), End Point Rate (EPR), Least Regression Rate (LRR), Weighted Least Squares Regression (WLR), Standard Error (LSE/WSE), R-squared (LR2/WR2), Least Median of Squares (LMS), and Jack-Knife Ratio (JKR). Each method has its own advantages and disadvantages (Thieler *et al*., 2003; Genz *et al*., 2007).

In this study, shoreline changes were predicted using two different statistical approaches: the EPR and LRR. In the EPR method, the calculation is performed by dividing the distance between the shoreline at the oldest and the most recent dates by the time elapsed (To and Thao, 2008). The equation for the calculated statistics is:

$$EPR = \frac{(d_1 - d_0)}{(t_1 - t_0)} \quad (1)$$

In the calculations, the statistical ratio is determined using two different shorelines. If there are more than two shorelines, this method is calculated using different combinations (Beyazıt *et al*., 2014). The LRR is determined by placing the most suitable regression line, based on the method of least squares, on all of the shoreline points for a certain transect. The equation for the calculated linear regression line is:

$$y = mx + b \quad (2)$$

Here, *m* is the slope of the line, *b* is a constant value, *x* is an independent variable, and *y* is a dependent variable (Thieler *et al.,* 2009). In this method, all shorelines are taken into account independently of changes in the tendency and accuracy (Mahapatra *et al*., 2014). The method is based on statistical concepts and is very easy to use. All statistical calculations in this study were performed with the data uncertainty of ±5 m and a confidence interval of 95%. As a result, the predicted shoreline change rates (erosion or accretion) at each transect were presented in graphs in Fig. 5. Due to the long shoreline in the study and the frequent transect range created (50 m), the study area was divided into 4 different regions, and statistical calculations were performed (Fig. 5).

### 2.3.4. Trend analysis

Trends arise as a result of a change in the values of a random variable that increases or decreases in a time-dependent manner. To perform statistical analysis in any data set to determine trends, the probability of occurrence of the observed data must be the same and independent of each other, and the observed variable must be observed under similar conditions, that is, it must be homogeneous. Generally, these data sets are affected by many events, such as the observation method, hydrological and meteorological events, human factors, etc. Therefore, they lose their randomness and their homogeneity deteriorates. Therefore, sufficient statistical results cannot be obtained to determine trends in data sets that are not homogeneous and do not show random variables (Çetin, 1997). In this study, the Run (Swed-Eisenhart) test was used as a homogeneity test to determine whether the data used to determine trends come from the

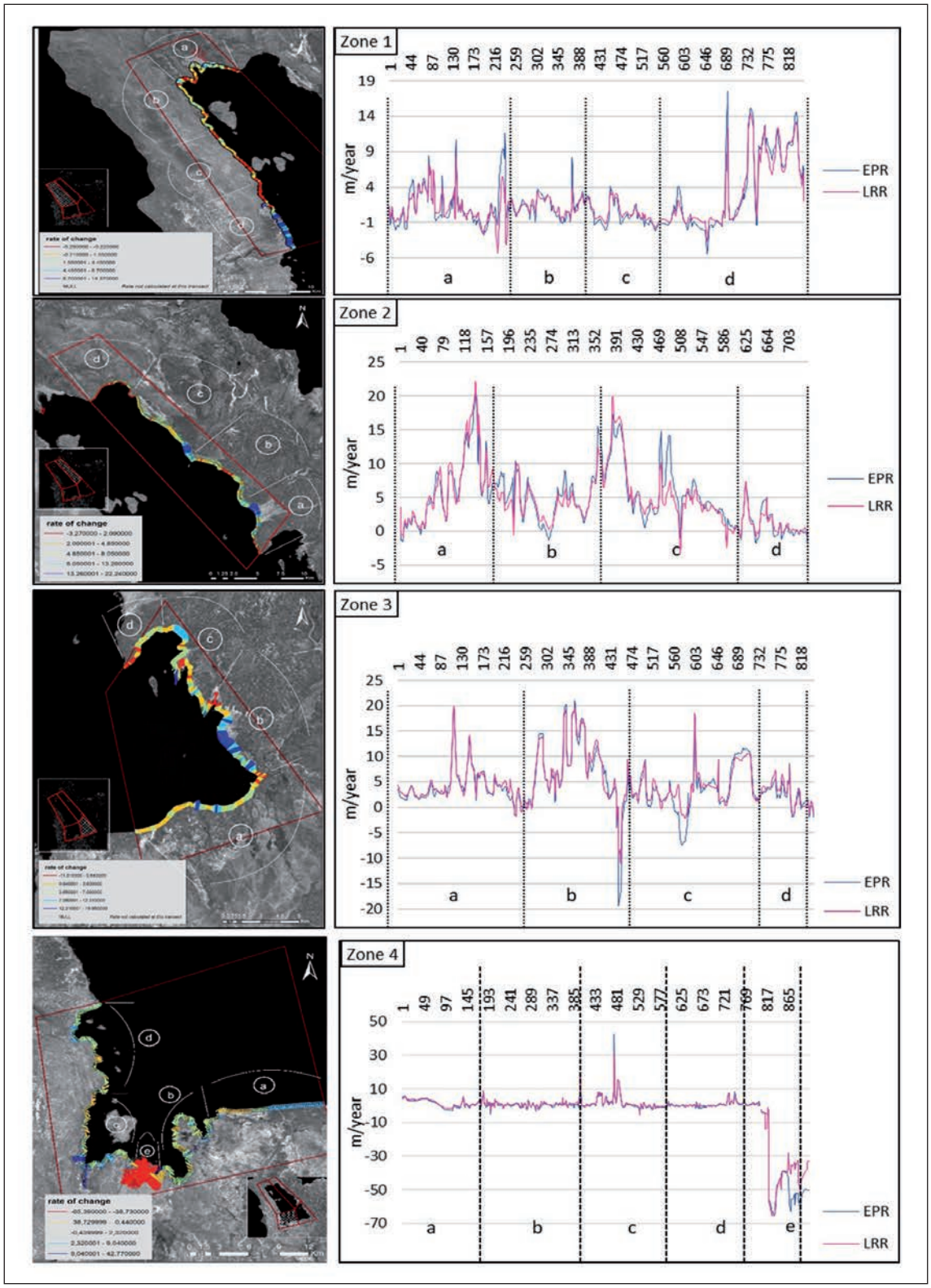


Fig. 5 - Shoreline change rates from zone 1 to zone 4 from 1984 to 2018.

same population and are independent of each other. In addition, to determine whether there is an internal dependency between the data, the autocorrelation coefficients test was performed before the Mann-Kendall test.

Mann-Kendall test. The existence of monotonous increasing or decreasing trends in the time series was tested with the non-parametric Mann-Kendall test. In the calculation of the Mann-Kendall statistical test, the *S* statistics for time series with less than 10 data points and the normal approximation (*Z*) statistics for time series with 10 or more data points are used (Gilbert, 1987). The variance of *S*, *VAR*(*S*), was calculated by:

$$VAR(S) = \frac{1}{18}\left[n(n-1)(2n+5) - \sum_{p=1}^{q} t_p(t_p-1)(2t_p+5)\right] \quad (3)$$

Here, *q* is the number of groups (*p*) that have equal value and $t_p$ is the number of data values in the *p-th* group. The normal approximation statistic value (*Z*) is calculated according to the values of *S* and *VAR*(*S*) given above, according to:

$$Z = \begin{cases} \frac{S-1}{\sqrt{VAR(S)}} & if\ S > 0 \\ 0 & if\ S = 0 \\ \frac{S+1}{\sqrt{VAR(S)}} & if\ S < 0 \end{cases} \quad (4)$$

Statistically, determining whether there is a trend in a time series is evaluated by looking at the value of the *Z* statistic. The absolute value of *Z* is compared with the *Z*1-α/2 value determined at the α significance level from the standard normal cumulative distribution tables. It is concluded that the trend exists if the absolute value of *Z* is greater than or equal to *Z*1-α/2. A positive value of *Z* indicates that there is an increasing trend and a negative value of *Z* indicates that there is a decreasing trend.

Sen Slope test. The non-parametric Sen Slope method is used to estimate the true slope of a nonlinear trend in a time series (as an annual change). One of the most important features of this method is that it is not greatly affected by single data errors or outlier measure values (Gilbert, 1987). To estimate the true slope (*Q*) of a time series, it is first necessary to calculate the slope (*QI*) of the data value pairs in the whole time series with the following equation as *j* > *k*:

$$Q_i = \frac{x_j - x_k}{j-k} \quad (5)$$

It is obtained by the number *N*[*n**(*n*-1)/2] from the $Q_i$ value showing the slope estimation according to the value *n* representing the number of *xj* in the time series. In the Sen slope method, the slope estimator of the trend is the median of *N* number of $Q_i$ values. To calculate this value, the $Q_i$ values are ordered from the smallest to the largest. Depending on whether *N* is odd or even, the estimator of the Sen Slope method was calculated using:

$$Q = Q_{[(N+1)/2]}, if\ N\ is\ odd$$
$$Q = \frac{1}{2}\left(Q_{[N/2]} + Q_{[(N+2)/2]}\right), if\ N\ is\ even. \quad (6)$$

The median of $Q_i$ values indicates the magnitude and direction of an existing trend in time series. In other words, if the sign of *Q* is negative (positive), it means that there is a decreasing (increasing) trend. The higher the value of *Q*, the more trends there are.

### 2.3.5. Drought analysis

Nowadays, drought is accepted as one of the natural disasters caused by factors such as rainfall below normal levels and the negative effects of climate change, etc. It is predicted that rainfall will decrease, temperatures will increase, and briefly, the severity of drought will increase and its duration will be extended in the future. In drought analyses, drought indices are calculated using the data obtained from meteorological, agricultural, and hydrological observations. The effect of drought on rainfall was determined in this study with the Standard Precipitation Index (SPI). It will also be interpreted whether the results affect time-dependent geometric shoreline changes in Lake Beyşehir.

Standardised Precipitation Index. The SPI was developed as a method that converts the rainfall parameter into a single numerical value for the purpose of monitoring the drought by Mckee *et al*. (1993). It is used as an effective solution for determining seasonal meteorological droughts by using monthly rainfall data with this method. However, the probability distribution function of precipitation data used in this method generally does not conform to a normal distribution. The probability distribution functions of these data need to be converted into Gamma probability distribution functions. After this transformation, precipitation data are brought to a normal distribution state by using the inverse standard normal distribution function. The SPI is obtained by dividing the standard deviation (σ) of difference by the mean (*Xiort*) of the precipitation (*Xi*) within a selected time period (Eq. 7). In this way, a SPI with a mean of 0 and a variance of 1 is calculated (McKee *et al*., 1993).

$$SPI = \frac{x_i - x_J}{\sigma} \tag{7}$$

Today, SPI calculations are made for different periods (1, 3, 6, 9, 12, and 24 months) to evaluate meteorological, agricultural, and hydrological droughts in the short or long term. In this study, the SPI values for 1, 9, 12, 24, and 60 months were calculated. For the detection of agricultural and hydrological droughts of longer periods, the 9-month SPI is an indicator of seasonal precipitation patterns over a medium-scale period. SPIs for 12 and 24 months are calculated to determine long-term precipitation patterns, and hydrological dry periods observed in streams, reservoir levels, and groundwater levels. The SPI compares all of the data with the amount of precipitation recorded over the same consecutive month in the previous 12-year period. In addition, 60-month (5-year) SPI values were also calculated in order to achieve parallelism with the satellite images (World Meteorological Organization, 2012) used to determine the coastal changes and to determine the drought periods. According to the obtained SPI values, evaluations were made by comparing the values given in Table 5 below and the type of drought was determined.

Table 5 - Drought category according to the SPI values (McKee *et al*., 1993).

| RANGE OF SPI VALUE | PRECIPITATION REGIME |
|---|---|
| ≥ 2 | Extremely wet |
| 1.50 ~ 1.99 | Very wet |
| 1.00 ~ 1.49 | Moderately wet |
| 0.99 ~ -0.99 | Normal precipitation |
| -1.00 ~ -1.49 | Moderately dry |
| -1.50 ~ -1.99 | Very dry |
| ≤ - 2 | Extremely dry |

## 3. Results and discussion

After performing a general assessment for each region (using all of the transects), examinations were also made for erosion and accretion. The total positive change movements of the transects, examined statistically in Table 6, indicate accretion, while the negative change movements indicate erosion rates.

Table 6 - Shoreline change trends, derived from the LRR and EPR, using the 4 zones.

| | ZONE 1 | | | | | | ZONE 2 | | | | | |
|---|---|---|---|---|---|---|---|---|---|---|---|---|
| **Transection Type** | **General** | | **Erosion** | | **Accretion** | | **General** | | **Erosion** | | **Accretion** | |
| **Methods** | **EPR** | **LRR** | **EPR** | **LRR** | **EPR** | **LRR** | **EPR** | **LRR** | **EPR** | **LRR** | **EPR** | **LRR** |
| **Number of values** | 849 | 849 | 344 | 291 | 505 | 558 | 737 | 737 | 79 | 48 | 658 | 689 |
| **Minimum** | -5.40 | -5.29 | -5.40 | -5.29 | 0.00 | 0.00 | -1.78 | -3.27 | -1.78 | -3.27 | 0.04 | 0.00 |
| **Maximum** | 17.49 | 14.37 | -0.01 | -0.01 | 17.49 | 14.37 | 21.35 | 22.24 | -0.01 | -0.02 | 21.35 | 22.24 |
| **Mean** | 1.94 | 1.88 | -1.08 | -0.79 | 3.99 | 3.27 | 4.92 | 4.74 | -0.63 | -0.53 | 5.59 | 5.11 |
| **Median** | 0.61 | 0.62 | -1.04 | -0.59 | 2.36 | 1.98 | 4.31 | 3.80 | -0.55 | -0.29 | 4.76 | 4.06 |
| **First quartile** | -0.80 | -0.34 | -1.44 | -0.95 | 1.00 | 0.67 | 1.50 | 1.70 | -0.99 | -0.59 | 2.56 | 2.29 |
| **Third quartile** | 3.02 | 2.65 | -0.54 | -0.31 | 6.50 | 4.35 | 7.09 | 6.13 | -0.24 | -0.15 | 7.47 | 6.31 |
| **Standard error** | 0.14 | 0.12 | 0.04 | 0.05 | 0.18 | 0.15 | 0.16 | 0.16 | 0.05 | 0.10 | 0.16 | 0.16 |
| **Variance** | 15.82 | 12.16 | 0.58 | 0.66 | 15.79 | 12.50 | 19.00 | 19.13 | 0.23 | 0.52 | 17.11 | 18.36 |
| **Average deviation** | 2.99 | 2.54 | 0.55 | 0.52 | 3.25 | 2.75 | 3.37 | 3.18 | 0.40 | 0.44 | 3.19 | 3.12 |

| | ZONE 3 | | | | | | ZONE 4 | | | | | |
|---|---|---|---|---|---|---|---|---|---|---|---|---|
| **Transection Type** | **General** | | **Erosion** | | **Accretion** | | **General** | | **Erosion** | | **Accretion** | |
| **Methods** | **EPR** | **LRR** | **EPR** | **LRR** | **EPR** | **LRR** | **EPR** | **LRR** | **EPR** | **LRR** | **EPR** | **LRR** |
| **Number of values** | 843 | 843 | 70 | 55 | 773 | 788 | 911 | 911 | 427 | 333 | 484 | 578 |
| **Minimum** | -19.38 | -11.01 | -19.38 | -11.01 | 0.02 | 0.00 | -65.39 | -65.44 | -65.39 | -65.44 | 0.00 | 0.00 |
| **Maximum** | 21.03 | 19.95 | -0.01 | -0.01 | 21.03 | 19.95 | 42.77 | 30.31 | -0.01 | -0.01 | 42.77 | 30.31 |
| **Mean** | 4.38 | 4.77 | -3.82 | -1.89 | 5.13 | 5.23 | -4.53 | -3.49 | -12.03 | -12.90 | 2.09 | 1.92 |
| **Median** | 3.50 | 3.79 | -1.73 | -1.07 | 3.74 | 3.93 | 0.12 | 0.37 | -0.97 | -0.85 | 1.17 | 1.07 |
| **First quartile** | 1.86 | 2.26 | -5.84 | -1.63 | 2.16 | 2.54 | -0.91 | -0.41 | -4.06 | -33.30 | 0.50 | 0.43 |
| **Third quartile** | 6.29 | 6.34 | -0.81 | -0.37 | 6.76 | 6.66 | 1.27 | 1.43 | -0.49 | -0.32 | 2.80 | 2.55 |
| **Standard error** | 0.17 | 0.15 | 0.59 | 0.37 | 0.15 | 0.15 | 0.54 | 0.47 | 1.03 | 1.09 | 0.14 | 0.11 |
| **Variance** | 24.47 | 19.41 | 24.15 | 7.68 | 17.87 | 16.93 | 265.63 | 200.70 | 450.49 | 398.31 | 9.42 | 6.88 |
| **Average deviation** | 3.47 | 3.21 | 3.54 | 1.71 | 3.22 | 3.10 | 9.57 | 8.30 | 17.17 | 17.18 | 1.76 | 1.64 |

Standard deviations were also investigated to compare the EPR and LRR methods in terms of coastal boundary changes, and evaluate the statistical analyses conducted (Fig. 6).

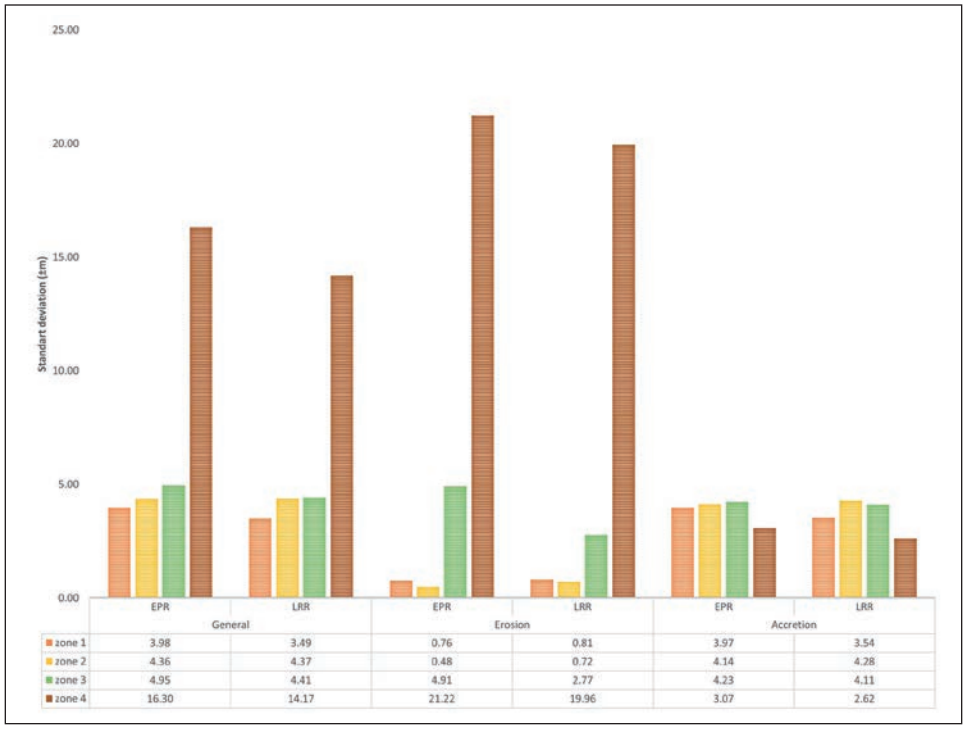


Fig. 6 - Standard deviations obtained from the EPR and LRR methods.

Upon examining the standard deviations in Fig. 6, it was observed that the LRR and EPR methods yielded results close to each other. Fig. 7 shows a comparative graph of the EPR and LRR methods. According to the regression analysis graph, it was seen that there was a 92% relationship between these two methods.

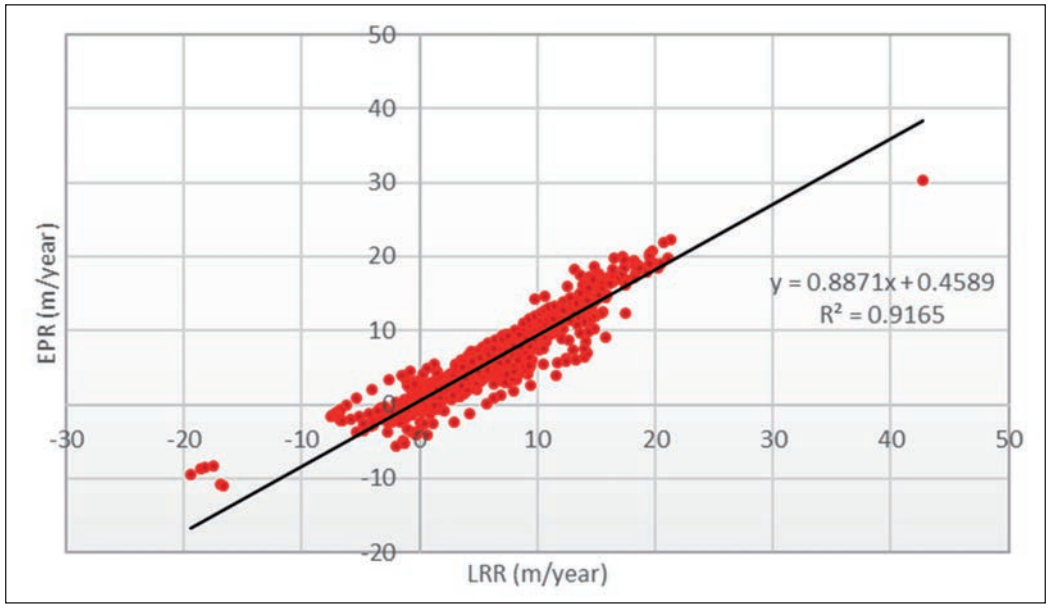


Fig. 7 - Regression graph of the EPR and LRR result values.

When the values obtained from the transects were compared, it was determined that the LRR method yielded more accurate results by showing less standard deviation in comparison with the EPR method. Therefore, the results of the LRR statistics were utilised in the interpretation section.

As a result of the applied statistical methods, it was concluded that there was a tendency toward accretion in the 1st region (NW axis), with a mean shoreline change rate of 1.88 m/yr (shoreline accretion of 65.65 m on average) and 849 transects along the 45-km shoreline. The average coastal erosion rate here of -0.79 m/yr (-36.76 m) covered 34% of the shoreline. The coastal accretion rate of 3.27 m/yr (136.1 m) covered 66% of the shoreline. Negative change movements were experienced less often than positive change movements in the region. The reason for this was that the presence of the Kızıldağ National Park, which is a slope mountainous area covering almost the whole of the NW axis shoreline, has prevented coastal erosion.

It was concluded that there was a tendency toward accretion in the 2nd region (NE axis), with a mean shoreline change rate of 4.74 m/yr (shoreline accretion of 126.5 m on average) and 737 transects along the 39-km shoreline. The average coastal erosion rate here of -0.53 m/yr covered 6.5% of the shoreline. The coastal accretion rate of 5.11 m/yr covered 93.5% of the shoreline. Negative change movements were experienced less often than positive change movements in the region.

It was concluded that there was a tendency toward accretion in the 3rd region (SE axis), with a mean shoreline change rate of 4.77 m/yr (shoreline accretion of 149.31 m on average) and 843 transects along the 44-km shoreline. The average coastal erosion rate here of -1.89 m/yr (-130.31 m) covered 6.5% of the shoreline. The coastal accretion rate of +5.23 m/yr (174.63 m) covered 93.5% of the shoreline.

It was concluded that there was a tendency toward erosion in the 4th region (SW axis), with a mean shoreline change rate of -3.49 m/yr (shoreline withdrawal of -154.11 m on average) and 911 transects along the 48-km shoreline. The biggest change in Lake Beyşehir was observed in this region. The average coastal erosion rate here of -12.90 m/yr (-407.41 m) covered 36.5% of the shoreline. The coastal accretion rate of 1.92 m/yr (71.4 m) covered 63.5% of the shoreline. The map of shoreline accretion and erosion is shown in Fig. 8.

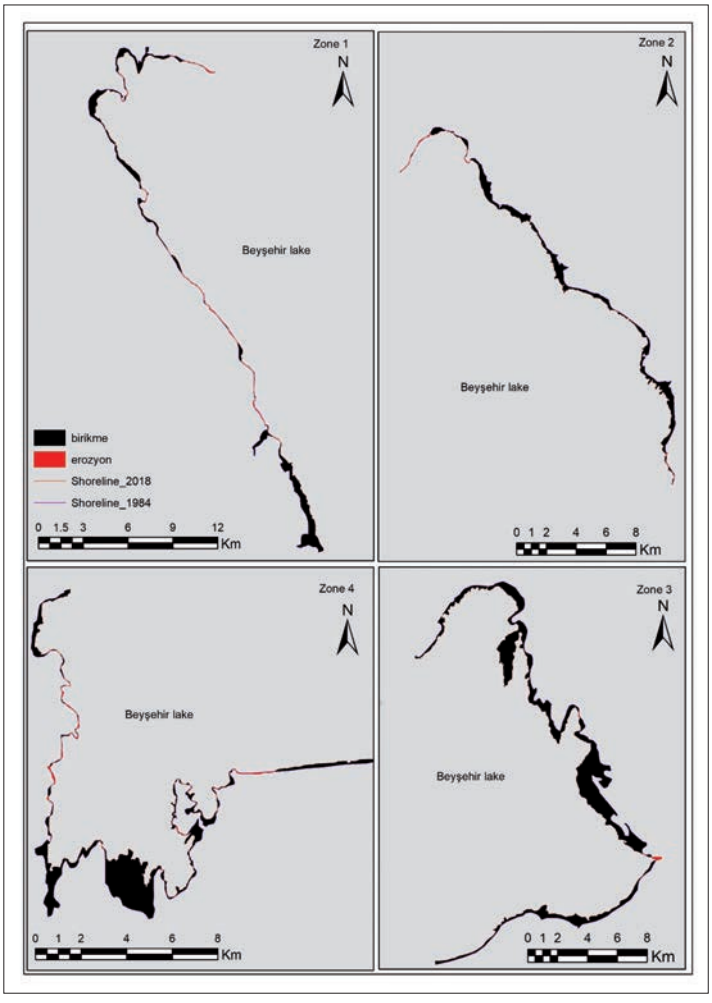


Fig. 8 - Accretion and erosion map on the coastline (1984-2018).

As a result of all of the analyses conducted, morphological changes were determined in the coastal lagoons located on the NW, NE, SW, and SE axes of Lake Beyşehir. It was determined that the most detected coastal problem in all of the regions was coastal accretion. Trend and drought analysis was applied to explain the main reason for this progress. The results were associated with each other and interpreted.

Before applying the trend analysis, Spearman Rho correlation analysis was conducted to determine the direction and size of the relationship between the annual average temperature and precipitation data for 1970 to 2018, obtained from the Beyşehir Meteorological Observation Station. The results obtained are given in Table 7.

Table 7 - Results of the Spearman Rho correlation analysis.

| Beyşehir Meteorological Data | | Minimum temperature | Average temperature | Maximum temperature | Total precipitation |
|---|---|---|---|---|---|
| Minimum temperature | coefficients | 1.000 | 0.771** | 0.254 | 0.154 |
| | sig. | | 0.000 | 0.078 | 0.290 |
| Average temperature | coefficients | 0.771** | 1.000 | 0.556** | 0.345* |
| | sig. | 0.000 | | 0.000 | 0.015 |
| Maximum temperature | coefficients | 0.254 | 0.556** | 1.000 | 0.158 |
| | sig. | 0.078 | 0.000 | | 0.279 |
| Total precipitation | coefficients | 0.154 | 0.345* | 0.158 | 1.000 |
| | sig. | 0.290 | 0.015 | 0.279 | |

** Correlation is significant at the 0.01 level. * Correlation is significant at the 0.05 level.

When Table 7 is examined, it is seen that there is a statistically significant positive relationship between the meteorological data. Correlation coefficients consist of values between 0 and 1 that measure the direction and amount of linear relationship between temperatures and precipitation data. It was concluded that there was a statistically significant relationship in the data where the values in the Asymp. Sig. (significance) line were less than 0.05.

In general, there was a statistically significant positive relationship between the temperatures and precipitation. It was observed that both the amount of precipitation and the temperatures decreased between 1970 and 2018.

Trend analysis was applied to determine whether there was a time-dependent change in the temperature and precipitation data observed from the Beyşehir station from 1970 to 2018. The homogeneity of the data and whether there was an autocorrelation between the data were determined before the analysis. Trends determined for the temperature and precipitation data using the non-parametric Mann-Kendall and Sen Slope tests are given in Table 8.

Table 8 - Values obtained from the Mann-Kendall and Sen Slope test for the Beyşehir Meteorological Observation Station data.

| Beyşehir Station | Mann- Kendall | | | | Sen's Slope | | | |
|---|---|---|---|---|---|---|---|---|
| Meteorological Data | S | Var(S) | Test Z | Trend-Direction | Q | Qmin | Qmax | Trend-Direction |
| minimum temperature | -22 | 13458.67 | -0.18 | NO | 0.00 | 0.00 | 0.00 | NO |
| average temperature | 210 | 13458.67 | 1.80 | NO | 0.00 | 0.00 | 0.00 | NO |
| maximum temperature | 554 | 13458.67 | 4.77 | YES (+) | 0.00 | 0.00 | 0.10 | NO |
| Total Precipitation | 224 | 13458.67 | 1.92 | NO | 0.20 | 0.00 | 0.30 | YES (+) |

When the results obtained by applying the Mann-Kendall and Sen Slope tests to the temperature and precipitation data were examined, an increasing trend was found in the time-dependent maximum temperature data in using Mann-Kendall test. In the other data, there were no time-dependent increasing or decreasing trends. In the Sen Slope test, an increasing time-dependent trend was obtained only in the precipitation data. In general, when the results obtained from both methods were compared, there was an increasing trend in the maximum temperature and precipitation data between 1970 and 2018.

In addition, the SPI values for the different time scales (1, 9, 12, 24, and 60 months) were calculated from the precipitation data of the Beyşehir Meteorological Station between for 1970 and 2018. Assessments were conducted for the meteorological, agricultural, and hydrological droughts in the short or long term. The drought periods obtained from the 9-, 12-, 24-, and 60-month SPI values, which are generally calculated for the detection of agricultural and hydrological droughts, are given in Table 9.

Table 9 - Drought periods calculated from the SPI values according to different time scales.

| | Drought Period | | | | | | |
|---|---|---|---|---|---|---|---|
| **Time Scale** | **Start_Date** | **End_Date** | **Duration** | **Peak** | **Sum** | **Average** | **Median** |
| 9 monthly | 1.01.1972 | 9.01.1972 | 8 | -2.32 | -11.26 | -1.41 | -1.59 |
| | 2.01.1974 | 1.01.1975 | 11 | -2.77 | -22.11 | -2.01 | -2.04 |
| | 10.01.1981 | 9.01.1983 | 23 | -2.29 | -27.35 | -1.19 | -1.12 |
| | 12.01.1984 | 11.01.1985 | 11 | -2.17 | -12.62 | -1.15 | -0.95 |
| | 11.01.1986 | 6.01.1987 | 7 | -2.45 | -5.81 | -0.83 | -0.61 |
| | 8.01.1989 | 11.01.1989 | 3 | -2.81 | -6.42 | -2.14 | -2.37 |
| | 8.01.2007 | 12.01.2007 | 4 | -2.11 | -5.92 | -1.48 | -1.82 |
| 12 monthly | 12.01.1971 | 2.01.1975 | 38 | -2.78 | -61.61 | -1.62 | -1.75 |
| | 12.01.1982 | 12.01.1983 | 12 | -2.11 | -17.46 | -1.45 | -1.51 |
| | 4.01.1985 | 11.01.1985 | 7 | -2.25 | -9.57 | -1.37 | -1.3 |
| 24 monthly | 12.01.1972 | 10.01.1976 | 46 | -3.18 | -70.15 | -1.52 | -1.74 |
| | 1.01.1983 | 4.01.1988 | 63 | -2.38 | -62.38 | -0.99 | -0.94 |
| | 12.01.1993 | 10.01.1995 | 22 | -2.21 | -23.14 | -1.05 | -1.06 |
| 60 monthly | 12.01.1974 | 1.01.1979 | 49 | -2.83 | -84.53 | -1.73 | -1.81 |
| | 11.01.1986 | 12.01.1991 | 61 | -2 | -45.14 | -0.74 | -0.52 |

A comparison of the drought conditions of the STI values for the different time scales (1, 9, 12, 24, and 60 months) to determine the effect of precipitation changes on time-dependent geometric coastline changes in Lake Beyşehir is given in Table 10. Drought periods were determined according to the acquisition dates of the satellite images used.

Table 10 - Drought conditions of the SPI values calculated according to the acquisition dates of the satellite images.

| **Satellite image** | **1 monthly** | | **9 monthly** | | **12 monthly** | | **24 monthly** | | **60 monthly** | |
|---|---|---|---|---|---|---|---|---|---|---|
| **acquisition dates** | **SPI** | **type** | **SPI** | **type** | **SPI** | **type** | **SPI** | **type** | **SPI** | **type** |
| 7.01.1984 | -1.41 | moderately dry | 0.14 | normal | 0.04 | normal | -1.03 | moderately dry | -0.19 | normal |
| 8.01.1990 | -1.62 | Very dry | -0.89 | normal | 0.38 | normal | -0.7 | normal | -0.2 | normal |
| 8.01.1996 | 0.37 | normal | 0.41 | normal | 1.32 | moderately wet | 1.61 | very wet | 0.31 | normal |
| 8.01.2000 | 0.8 | normal | -0.44 | normal | -1.21 | moderately dry | 0.65 | normal | 0.99 | normal |
| 8.01.2006 | 0.31 | normal | -0.73 | normal | 0.07 | normal | -0.8 | normal | 0.59 | normal |
| 7.01.2014 | 0.75 | normal | 0.21 | normal | 0.02 | normal | 0.39 | normal | 1.11 | moderately wet |
| 8.01.2018 | -0.76 | normal | -0.75 | normal | -0.18 | normal | 0.25 | normal | 0.1 | normal |

Drought periods were indicated between the years when the coastal boundary changes in Lake Beyşehir were examined in Table 10. Drought was detected in the months covering this period from 1983 to 1996. The drought conditions covering the dates when satellite images were obtained are shown in Table 11. The drought conditions obtained according to the SPI values in different scales were evaluated in general. Near-normal drought conditions were detected on the dates of shooting the satellite photographs covering 1984, 1990, 1996, and 2000. In the month covering 2014, it was determined that there was a period of almost normal rainfall.

The water level and area of the lake Beyşehir changed between 1984 and 2018 as a result of the erosion and accretions in Beyşehir Lake. This change gave meaningful results according to the analysis made with precipitation and temperature data. Coastal change information for the lake surface area is given in Fig. 9. The area of the lake decreased between 1984 and 2006 as a result of the precipitation and temperatures. It was determined that the lake surface area increased due to nearly normal rainfall in the time period between 2006 and 2018. In addition, time-dependent coastal changes were in line with the results of the drought analysis.

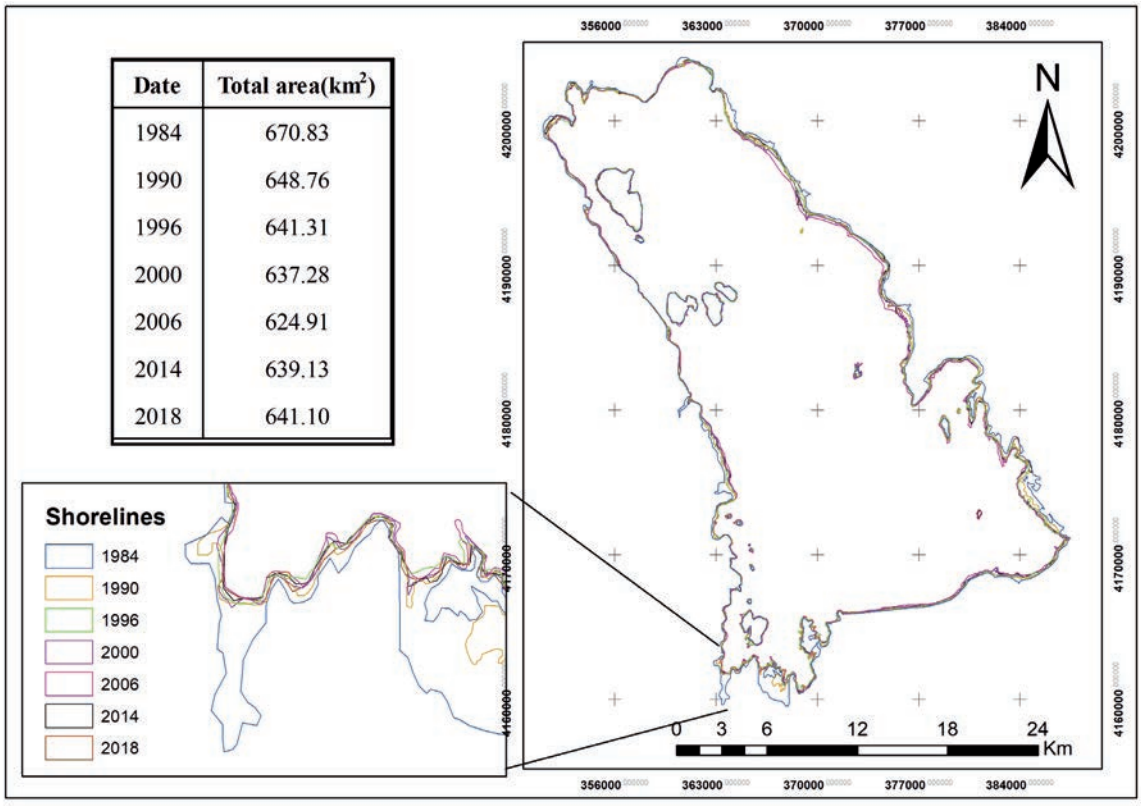


Fig. 9 - Beyşehir Lake surface area change by year.

## 4. Conclusions

The coastline changes were investigated by using Landsat satellite images obtained on 7 different dates (approximately every 5 years), between 1984 and 2018, in Lake Beyşehir, which is the largest freshwater reserve in Turkey, using an RS and GIS-based approach. The EPR and LRR statistical analysis methods were used to determine the erosion and accretion rates. According to the analysis results, the average coastal erosion rate was -12.03 m/yr with a shoreline recession of 409.06 m, while the average coastal accretion rate was 5.86 m/yr with a shoreline advance of 178.36 m, which were determined over a period of 35 years. The maximum coastal erosion rate was 42.77 m/yr with shoreline recession of 1457.55 m, while the maximum coastal accretion rate was 65.39 m/yr with a coastline advance of 2304.52 m, which were determined for the maximum variations. As a result of all the analyses conducted, it was determined that the change movements in the coastline, such as coastal erosion and accretion, were morphological changes in the coastal lagoons located on the NW, NE, SW, and SE axes of Lake Beyşehir. It was determined that the most detected coastal problem in all of the regions was coastal progression.

In addition, correlation, trend, and drought analyses were applied to the temperature and precipitation data to understand the reasons for the coastal boundary changes in Beyşehir Lake. Spearman Rho correlation analysis was conducted to determine the direction and size of the relationship between the annual average temperature and precipitation data for 1970 to 2018, obtained from the closest Beyşehir Meteorological Observation Station,

in the study area. As a result of the analysis, it was determined that there was a statistically significant positive relationship between the meteorological data, wherein both the amount of precipitation and the temperatures increased. The trend and the direction of the trend were determined using the non-parametric Mann-Kendall and Sen Slope tests. An increasing trend was found in the time-dependent maximum temperature data in the Mann-Kendall test. In the other data, there were no increasing or decreasing time-dependent trends. In the Sen Slope test, an increasing time-dependent trend was obtained only in the precipitation data. When the results obtained from these two methods were evaluated, there was an increasing trend in the maximum temperature and precipitation data between 1970 and 2018 in general.

In addition, the SPI values for the different time scales (1, 9, 12, 24, and 60 months) were calculated from the precipitation data of the Beyşehir Meteorological Observation Station between 1970 and 2018. Assessments have been made for meteorological, agricultural, and hydrological droughts in the short or long term. The periods when the coastal boundary changes in Lake Beyşehir were examined and the drought periods were compared. During the months covering this period from 1983 to 1996, drought was detected in general. Near-normal drought conditions were detected on the date of shooting satellite photographs covering 1984, 1990, 1996, and 2000. It was determined that there was an almost normal rainy period in the month covered in 2014.

The water level and area of the lake changed between 1984 and 2018 as a result of the erosion and accretions in Beyşehir Lake. These changes gave meaningful results according to the analysis made with precipitation and temperature data. The surface area of Beyşehir Lake decreased between 1984 and 2006 as a result of precipitation and temperatures. It was determined that the surface area of the lake increased due to nearly normal rainfall in the time period between 2006 and 2018.

Upon evaluating the study in general, it was observed that Lake Beyşehir was exposed to various changes, such as erosion and accretion of the shoreline under the effect of physical, climatic, and human factors in the 35-year period (1984 and 2018). To reduce these effects, it is necessary to review the existing policies of the local government for the protection and management of the existing and limited land resources in the study area, and to prepare more comprehensive planning activities in this regard. All legal regulations, analyses, and inquiries regarding the coastal zone management in developed countries are conducted using GIS and RS technologies. In this way, while the natural structure is planned in a sustainable manner, the socio-economic structure is also developed in a sustainable manner in long-term plans. The results of this study have also demonstrated that DSAS, which is a tool integrated into GIS, can provide important information about the morphodynamical behaviour of shorelines in the determination of temporal and geometric changes in the shoreline and erosion and accretion areas. Finally, the Landsat satellite images used in the study were medium spatial resolution images and were not in the class of high-resolution satellite images. Therefore, high-resolution satellite images should be used to minimise the margin of error in shoreline changes.

**Acknowledgments.** This work was supported by the Necmettin Erbakan University Scientific Research Projects Unit (grant numbers 191419002). We also thank the United States Geological Research Institute (USGS) for supplying the Landsat satellite imagery used in the study.

REFERENCES

Ahmad S.R. and Lakhan V.C.; 2012: *GIS-based analysis and modeling of coastline advance and retreat along the coast of Guyana*. Mar. Geod., 35, 1-15.

Alesheikh A.A., Ghorbanali A. and Nouri N.; 2007: *Coastline change detection using remote sensing*. Int. J. Environ. Sci. Technol., 4, 61-66, doi: 10.1007/BF03325962.

Ali P.Y. and Narayana A.C.; 2015: *Short-term morphological and shoreline changes at Trinkat Island, Andaman and Nicobar, India, after the 2004 tsunami*. Mar. Geod., 38, 26-39, doi: 10.1080/01490419.2014.908795.

Bagli S. and Soille P.; 2003: *Morphological automatic extraction of coastline from panEuropean Landsat ETM+ images.* In: Proc. 5th International Symposium on GIS and Computer Cartography for Coastal Zone Management, Genova, Italy, pp. 58-69.

Baral R., Pradhan S., Samal R.N. and Mishra S.K.; 2018: *Shoreline change analysis at Chilika lagoon coast, India using digital shoreline analysis system*. J. Indian Soc. Remote Sens., 46, 1637-1644.

Beyazıt I., Öztürk D. and Kılıç F.; 2014: *Kızılırmak deltası kıyı çizgisinin zamansal değişimi.* In: Proc. 5th Remote Sensing and Geographic Information Systems Symposium, Istanbul, Turkey, 10 pp., <www.uzalcbs2014. sempozyumu. net/bildiriler.php>.

Bheeroo R.A., Chandrasekar N., Kaliraj S. and Magesh N.S.; 2016: *Shoreline change rate and erosion risk assessment along the Trou Aux Biches-Mont Choisy beach on the northwest coast of Mauritius using GIS-DSAS technique*. Environ. Earth Sci., 75, 444, doi: 10.1007/s12665-016-5311-4.

Braud D.H. and Feng W.; 1998: *Semi-automated construction of the Louisiana coastline digital land/water boundary using Landsat Thematic Mapper satellite imagery*. Applied Oil Spill Research and Development Program (OSRAPD), Department of Geography and Anthropology, Louisiana State University, Baton Rouge, LA, USA, Tech. Rep. Ser. 97-002.

Çetin M.; 1997: *Some preliminary statistical analysis techniques and applications in hydrological data analysis*. DSİ Tech. Bull., 86, 53-63.

Chen L.C. and Rau J.Y.; 1998: *Detection of shoreline changes for tide-land areas using multi-temporal satellite images.* Int. J. Remote Sens., 19, 3383-3397.

Constanza R., d'Agre R., de Groot R., Farber S., Grasso M., Hannon B., Limburg K., Naeem R., O'Neill V., Paruelo J., Raskin R.G., Sutton P. and van den Belt M.; 1997: *The value of the world's ecosystem services and natural capital.* Nature, 387, 253-260, doi: 10.1038/387253a0.

Dereli M.A. and Tercan E.; 2020: *Assessment of shoreline changes using historical satellite images and geospatial analysis along the Lake Salda in Turkey*. Earth Sci. Inf., 13, 709-718.

Durduran S.S. and Çiftçi Ç.; 2008: *Bütünleşik kıyı alanları yönetimi (BKAY) ve Coğrafi Bilgi Sistemlerinin Rolü: Beyşehir Gölü Örneği.* In: Proc. 2nd Remote Sensing and Geographic Information Systems Symposium, pp. 398-405.

Duru U.; 2017: *Shoreline change assessment using multi-temporal satellite images: a case study of Lake Sapanca, NW Turkey*. Environ. Monit. Assess., 189, 385, doi: 10.1007/s10661-017-6112-2.

El Banna M. and Hereher M.E.; 2009: *Detecting temporal shoreline changes and erosion/accretion rates, using remote sensing, and their associated sediment characteristics along the coast of north Sinai, Egypt*. Environ. Geol., 58, 1419-1427, doi: 10.1007/s00254-008-1644-y.

El-Asmar H.M. and Hereher M.E.; 2011: *Change detection of the coastal zone east of the Nile Delta using remote sensing.* Environ. Earth Sci., 62**,** 769-777, doi: 10.1007/s12665-010-0564-9.

Esmail M., Mahmod W.E. and Fath H.; 2019: *Assessment and prediction of shoreline change using multi-temporal satellite images and statistics: case study of Damietta coast, Egypt.* Appl. Ocean Res., 82, 274-282.

Esteves L.S., William J.J., Nock A. and Lymbery G.; 2009: *Quantifying shoreline changes along the Sefton coast (UK) and the implications for research-informed coastal management.* J. Coastal Res., 56, 602-606.

Frazier P.S. and Page K.J.; 2000: *Water body detection and delineation with Landsat TM data.* Photogramm. Eng. Remote Sens., 66, 1461-1467.

Genz A.S., Fletcher C.H., Dunn R., Frazer L.N. and Rooney J.J.; 2007: *The predictive accuracy of shoreline change rate methods and alongshore beach variation on Maui, Hawaii*. J. Coastal Res., 23, 87-105, doi: 10.2112/05-0521.1.

Gilbert R.O; 1987: *Statistical methods for environmental pollution monitoring*, Wiley, New York, NY, USA, 336 pp.

Himmelstoss E.A.; 2009: *DSAS 4.0 - Installation instructions and user guide*. In: Thieler E.R., Himmelstoss E.A., Zichichi J.L. and Ergul A. (eds), The Digital Shoreline Analysis System (DSAS) Version 4.0 - An ArcGIS extension

for calculating shoreline change: U.S. Geological Survey, Reston, VA, USA, Open-File Report 2008-1278, ver. 4.2, 81 pp., <pubs.usgs.gov/of/2008/1278/>.

Hovsepyan A., Tepanosyan G., Muradyan V., Asmaryan S., Medvedev A. and Koshkarev A.; 2019: *Lake Sevan shoreline change assessment using multi-temporal Landsat images.* Geog. Environ. Sustainability, 12, 212-229, doi: 10.24057/2071-9388-2019-46.

Immanuvel David T. , Mukesh M.V., Kumaravel S. and Sabeen H.M.; 2016: *Long-and short-term variations in shore morphology of Van Island in Gulf of Mannar using remote sensing images and DSAS analysis.* Arabian J. Geosci., 9, 756, doi: 10.1007/s12517-016-2772-4.

Jayson-Quashigah P.N., Addo K.A. and Kodzo K.S.; 2013: *Medium resolution satellite imagery as a tool for monitoring shoreline change*. *Case study of the eastern coast of Ghana*. J. Coastal Res., 65, 511-516.

Kadıoğlu Y., Güner Ö. and Özkan G.; 2019: *Coastline change (1964-2014) in the Kocadere Delta (Muğla/Ören).* J. Int. Social Res., 12, 379-385, doi: 10.17719/jisr.2019.3835.

Kale M.M.; 2018: *Historical shoreline change assessment using DSAS: a case study of Lake Akşehir, SW Turkey*. In: Doğan A. and Gönüllü G. (eds), Current Debates in Sustainable Architecture, Urban Design & Environmental Studies, IJOPEC, London, UK, pp. 187-196.

Kale M.M., Ataol M. and Tekkanat İ.S.; 2019: *Assessment of shoreline alterations using a Digital Shoreline Analysis System: a case study of changes in the Yeşilırmak Delta in northern Turkey from 1953 to 2017.* Environ. Monit. Assess., 191, 398, doi: 10.1007/s10661-019-7535-8.

Kaliraj S., Chandrasekar N. and Magesh N.S.; 2014: *Impacts of wave energy and littoral currents on shoreline erosion/accretion along the south-west coast of Kanyakumari, Tamil Nadu using DSAS and geospatial technology.* Environ. Earth Sci., 71, 4523-4542, doi: 10.1007/s12665-013-2845-6.

Kayadibi O. and Aydal D.; 2013: *Quantitative and comparative examination of the spectral features characteristics of the surface reflectance information retrieved from the atmospherically corrected images of Hyperion*. J. Appl. Remote Sens., 7, 073528.

Kenea N.H.; 1997: *Digital enhancement of Landsat data, spectral analysis and GIS data integration for geological studies of the Derudeb area, southern Red Sea Hills, NE Sudan*. Selbstverlag Fachbereich Geowissenschaften, FU Berlin, Germany, 116 pp.

Kılar H. and Çiçek İ.; 2018: *Shoreline change analysis in Göksu Delta by using DSAS*. J. Geog. Sci., 16, 89-104, doi: 10.1501/Cogbil_0000000192.

Kuleli T.; 2010: *Quantitative analysis of shoreline changes at the Mediterranean Coast in Turkey.* Environ. Monit. Assess., 167, 387-397, doi: 10.1007/s10661-009-1057-8.

Kuleli T., Guneroglu A., Karsli F. and Dihkan M.; 2011: *Automatic detection of shoreline change on coastal Ramsar wetlands of Turkey*. Ocean Eng., 38, 1141-1149.

Kumar A., Narayana A.C. and Jayappa K.S.; 2010: *Shoreline changes and morphology of spits along southern Karnataka, west coast of India: a remote sensing and statistics-based approach.* Geomorphol., 120**,** 133-152.

Li R., Di K. and Ma R.; 2003: *3-D shoreline extraction from IKONOS satellite imagery*. Mar. Geod., 26, 107-115, doi: 10.1080/01490410306699.

Liu H. and Jezek K.C.; 2004: *Automated extraction of coastline from satellite imagery by integrating Canny edge detection and locally adaptive thresholding methods.* Int. J. Remote Sens., 25, 937-958, doi: 10.1080/0143116031000139890.

Lutgens F.K., Tarbuck E.J. and Tasa D.G; 2012: *Essentials of Geology, 11th ed.* Pearson Education, Upper Saddle River, NJ, USA, 576 pp.

Mahapatra M., Ratheesh R. and Rajawat A.S.; 2014: *Shoreline change analysis along the coast of south Gujarat, India, using digital shoreline analysis system.* J. Indian Soc. Remote Sens., 42, 869-876, doi: 10.1007/s12524-013-0334-8.

Mas J.F.; 1999: *Monitoring land-cover changes: a comparison of change detection techniques.* Int. J. Remote Sens., 20, 139-152.

McKee T.B., Doesken N.J. and Kleist J.; 1993: *The relationship of drought frequency and duration to time scales.* In: Proc. 8th Conference on Applied Climatology, American Meteorological Society, Anaheim, CA, USA, pp. 179-184.

Mohsen A., Elshemy M. and Zeidan B.A.; 2018: *Change detection for Lake Burullus, Egypt using remote sensing and GIS approaches*. Environ. Sci. Pollut. Res., 25, 30763-30771.

Moussaid J., Fora A.A., Zourarah B., Maanan M. and Maanan M.; 2015: *Using automatic computation to analyze the rate of shoreline change on the Kenitra coast, Morocco.* Ocean Eng., 102, 71-77.

Mutaqin B.W.; 2017: *Shoreline changes analysis in Kuwaru coastal area, Yogyakarta, Indonesia: an application of the Digital Shoreline Analysis System (DSAS).* Int. J. Sustainable Dev. Plann., 12, 1203-1214, doi: 10.2495/SDP-V12-N7-1203-1214.

Nassar K., Mahmod W.E., Fath H., Masria A., Nadaoka K. and Negm A.; 2019: *Shoreline change detection using DSAS technique: case of north Sinai coast, Egypt.* Mar. Georesour. Geotechnol., 37, 81-95.

Natesan U., Thulasiraman N., Deepthi K. and Kathiravan K.; 2013: *Shoreline change analysis of Vedaranyam coast, Tamil Nadu, India*. Environ. Monit. Assess., 185, 5099-5109, doi: 10.1007/s10661-012-2928-y.

Navrajan T., Biradar R.S., Madhavi P. and Sunit C.; 2005: *A study on shoreline changes of Mumbai coast using remote sensing and GIS.* J. Indian Soc. Remote Sens., 33, 85-91, doi: 10.1007/BF02989995.

Niya A.K., Alesheikh A.A., Soltanpor M. and Kheirkhahzarkesh M.M.; 2013: *Shoreline change mapping using remote sensing and GIS*. Int. J. Remote Sens. Appl., 3, 102-107.

Orhan O.; 2014: *Konya Kapalı Havzası'nda uzaktan algılama ve CBS teknolojileri ile iklim değişikliği ve kuraklık analizi*. Master's Thesis, Aksaray University, Institute of Science, Aksaray, Turkey, 96 pp. <hdl.handle.net/20.500.12451 /1832>.

Pardo-Pascual J.E., Almonacid-Caballer J., Ruiz L.A. and Palomar-Vazquez J.; 2012: *Automatic extraction of shorelines from Landsat TM and ETM multi-temporal images with subpixel precision.* Remote Sens. Environ., 123**,** 1-11.

Pepe G. and Coutu G.; 2008: *Beach morphology change study using ArcGIS spatial analyst.* Middle States Geog., 41, 91-97.

Pritam C. and Prasenjit A.; 2010: *The Shoreline change and sea level rise along coast of Bhitarkanika wildlife sanctuary, Orissa: an analytical approach of remote sensing and statistical techniques.* Int. J. Geomatics Geosci., 1, 436-455.

Rio L.D., Gracia J.F. and Benavente J.; 2013: *Shoreline change patterns in sandy coasts. A case study in SW Spain*. Geomorphol., 196**,** 252-266, doi: 10.1016/j.geomorph.2012.07.027.

Ryu J.-H., Won J.-S. and Min K.D.; 2002: *Waterline extraction from Landsat TM data in a tidal flat: a case study in Gosmo Bay, Korea.* Remote Sens. Environ., 83**,** 442-456.

Segal D.B.; 1983: *Use of Landsat multispectral scanner data for definition of limonitic exposures in heavily vegetated areas.* Econ. Geol., 78**,** 711-722, doi: 10.2113/gsecongeo.78.4.711.

Thanikachalam M. and Ramachandran S.; 2003: *Shoreline and coral reef ecosystem changes in Gulf of Mannar, southeast coast of India.* J. Indian Soc. Remote Sens., 31, 157-173, doi: 10.1007/BF03030823.

Thieler E.R., Martine D. and Ergui A.; 2003: *Tutorial for the Digital Shoreline Analysis System (DSAS)-Extension for ArcView*. Open File Report 03-076, USGS, Reston, U.S.A.

Thieler E.R., Himmelstoss E.A., Zichichi J.L. and Ergul A.; 2009: *The Digital Shoreline Analysis System (DSAS) Version 4.0 - An ArcGIS extension for calculating shoreline change.* Open-File Report 2008-1278, U.S. Geological Survey, Reston, VA, USA, doi: 10.3133/ofr20081278.

To D.V. and Thao P.T.P.; 2008: *A shoreline analysis using DSAS in Nam Dinh coastal area*. Int. J. Geoinf., 4, 37-42.

Tüstaş (Tüstaş Industrial Facilities a.s. Project Department); 1999: *Beyşehir Gölü sulak Alanı yüzey su toplama havzası yönetim planı analitik etüd raporu*. Cilt 1,2,3,4,5 Governorship of Konya and Beyşehir District Government, Ankara, Turkey, 142 pp.

United States Geological Research Institute; 2020: <https://Earthexplorer.usgs.gov/>.

World Meteorological Organization; 2012: *Standardized Precipitation Index user guide*. WMO1090, WMO, Geneva, Switzerland, 16 pp.

Corresponding author: Münevver Gizem Gümüs
Department of Geomatics Engineering, Faculty of Engineering, Niğde Ömer Halisdemir University
Alparslan Turkes street, Central campus, Niğde,Turkey
Phone: +90 388 225 4643; email: gizemkisaaga@ohu.edu.tr